

VICTORIA UNIVERSITY
MELBOURNE AUSTRALIA

Multifunctional PA6 composites using waste glass fiber and green metal organic framework/graphene hybrids

This is the Published version of the following publication

Unnikrishnan, Vishnu, Zabihi, Omid, Li, Quanxiang, Ahmadi, Mojtaba, Ferdowsi, Mahmoud Reza Ghandehari, Kannangara, Thathsarani, Blanchard, Patrick, Kiziltas, Alper, Joseph, Paul and Naebe, Minoo (2022) Multifunctional PA6 composites using waste glass fiber and green metal organic framework/graphene hybrids. *Polymer Composites*, 43 (9). pp. 5877-5893. ISSN 0272-8397

The publisher's official version can be found at
<https://4spepublications.onlinelibrary.wiley.com/doi/10.1002/pc.27002>
Note that access to this version may require subscription.

Downloaded from VU Research Repository <https://vuir.vu.edu.au/46100/>

Multifunctional PA6 composites using waste glass fiber and green metal organic framework/graphene hybrids

Vishnu Unnikrishnan¹ | Omid Zabihi¹ | Quanxiang Li¹ | Mojtaba Ahmadi¹ |
Mahmoud Reza Ghandehari Ferdowsi¹ | Thathsarani Kannangara² |
Patrick Blanchard³ | Alper Kiziltas³ | Paul Joseph² | Minoo Naebe¹ 

¹Institute for Frontier Materials, Carbon Nexus, Deakin University, Geelong, Victoria, Australia

²Institute for Sustainable Industries and Liveable Cities, Victoria University, Melbourne, Victoria, Australia

³Research and Product Development, Ford Motor Company, Dearborn, Michigan, USA

Correspondence

Minoo Naebe, Institute for Frontier Materials, Carbon Nexus, Deakin University, Geelong, VIC 3216, Australia.
Email: minoo.naebe@deakin.edu.au

Funding information

Australian Research Council Training Centre for Light Weight Automotive Structures (ATLAS), Grant/Award Number: IC160100032

Abstract

Glass fiber-polyamide 6 (PA6) composites are widely used for various automotive applications, yet the ability to exhibit multifunctional properties and the cost of it remains challenging. Herein this work introduces a cost-effective approach for utilization of waste glass fiber (GF), green aluminium metal organic framework (Al-MOF), and industry-grade graphene nanoplatelets (GNPs) for the fabrication of multifunctional PA6 thermoplastic composites with enhanced mechanical performance and fire retardancy. The results demonstrate that hybrid filler of Al-MOF and GNPs have a synergistic effect in improving the mechanical properties and fire retardancy of GF reinforced PA6 composites. Compared to the neat PA6, the PA6 composite containing 20 wt% GFs, 5 wt% GNPs, and 5 wt% Al-MOF exhibited ~97% and ~93% improvements in tensile and flexural strength, respectively. Also, compared to the neat PA6, 27 and 55°C increases were observed in glass transition temperature (T_g) and heat deflection temperature, respectively. Thermal stability and fire retardancy of the GFs/PA6 composites were significantly improved when hybridized with GNPs and Al-MOF.

KEYWORDS

mechanical properties, nanocomposites, recycling, thermoplastics, waste

1 | INTRODUCTION

Polyamide 6 (PA6) is an important class of engineering thermoplastic polymers widely used in automotive applications due to their excellent mechanical properties, toughness, elasticity, chemical resistivity, high melting points, and moldability.^[1,2] Conversely, properties such as chemical resistance, abrasion resistance, good

processability, and biocompatibility drive the novel polyamides toward development of sustainable composites structures.^[3] Hence, to reduce the cost and lead sustainable development, automotive industries utilize PA6 for a wide range of applications such as tubing, piping, injectors, manifolds, fuel tanks, and so forth.^[4,5] Recently, to improve the performance of PA6, it has been identified that the performance of PA6 polymer strongly depends

This is an open access article under the terms of the [Creative Commons Attribution-NonCommercial-NoDerivs](https://creativecommons.org/licenses/by-nc-nd/4.0/) License, which permits use and distribution in any medium, provided the original work is properly cited, the use is non-commercial and no modifications or adaptations are made.

© 2022 The Authors. *Polymer Composites* published by Wiley Periodicals LLC on behalf of Society of Plastics Engineers.

on the microstructural features such as crystallinity, phase content, and lamellar thickness, which is traditionally determined during processing. The effect of processing parameters on the inherent properties of PA6 can be further attributed to its physical and chemical structure.^[6] Still, factors such as hygroscopicity and plasticization^[7] lead to degradation of PA6's mechanical properties as noted in various literature.^[8–10] Therefore, to address this challenge, recent efforts have been directed toward employing reinforcing materials such as short glass fibers (SGFs)^[11] and short carbon fibers (SCFs).^[12] Currently, researchers have utilized recycled glass fibers (GFs) and carbon fibers as a reinforcing filler alongside PA6 polymers to improve mechanical and thermal properties.^[13,14]

¹ Also, it can be observed that the reinforcement of SCFs and SGFs purely enhances the mechanical properties of the thermoplastic composites, but underlying problems related to poor flame retardant characteristics remain a challenge. Given the importance of flame resistance performance in the modern composites market,^[15] the need to introduce fillers which can both maintain the mechanical integrity and simultaneously improve the flame resistance property becomes significantly important.^[16,17]

In this work, to improve the flame retardancy of pure PA6 thermoplastic composites, various flame retardant materials have been explored^[18–20] and consequently, novel fillers such as graphene and MOF have been studied. Graphene^[21] is a 2D material which has revolutionized the materials science industry owing to its unique chemical, thermal, mechanical, and physical properties.^[22,23] Flame retardant properties of graphene have attracted attention in recent years^[24] owing to its ability to form dense char layers during the fire growth, which helps in suppression of the degradation process of the polymer. This phenomenon has been elucidated by Huang et al.,^[25] who demonstrated that the addition of graphene nanosheets alongside poly(vinyl alcohol) improves the flame retardant properties such as peak heat release rate (pHRR) by 49%. Similarly, recent works on MOFs^[26,27] with various polymers highlights the potential of MOFs toward polymer composites with flame retardant characteristics.^[28] However, MOFs synthesis and bulk production of MOFs still remains the challenge.^[29] Therefore, to reduce the cost and improve multiverse of functional properties, green MOFs^[30–33] have been explored recently.

To develop thermoplastic composites with improved mechanical and flame retardant behavior, a novel strategy needs to be employed where improvement in reinforced polymers inherent performance can be achieved by employing fillers and fibers.^[34] It has been shown that incorporation of hybrid fillers-fibers into the polymer matrix improves wettability.^[35–37] The study by Unal and

Mimaroglu,^[38] showcased that the addition of 10% lamellar particle mica fillers alongside the 20% short GFs when reinforced with PA6 polymers improved the tensile strength and modulus. It was observed that the addition of GFs improved the flexural strength and modulus, however, increasing the addition of mica particles does not impact the flexural properties. Similar trend was observed in the tensile properties, and this was attributed to the increased insensitivity upon the addition of mica nanoparticles. In another study^[39] the addition of hybrids nano-aluminium oxide and graphene oxide (GO) to PA6 via melt blending improved the interfacial interactions in PA6 polymer composites, resulting in enhanced thermal conductivity. Additionally, Kim et al. studied the effect of dispersing various nanomaterials (multi-walled carbon nanotubes, GO and GNPs) in polyamide 66 (PA66). It was observed that the addition of 1:1 hybrid filler (GO and multiwalled carbon nanotubes) improved mechanical properties by 26.3%, 1.3% Young's modulus and tensile strength respectively when compared to pristine PA66. Sabet et al.^[40] also exhibited that the addition of 4%wt loading of graphene in PA6 enhanced the fire retardancy. Here, the heat release rate (HRR), carbon monoxide production (COP) and total heat release (THR) decreased by 32%, 38%, and 16% respectively. Recently, tannin acid has been utilized alongside metal oxide nanoparticle to improve the mechanical and flame retardancy of the composites.^[41–44]

MOFs inclusion in PA6 has been explored for applications in membranes, where Wang et al.,^[45] showcased incorporation of zirconium (Zr-) based MOF leading to improved mechanical performance due to the hydrogen bonds interaction between MOFs and PA6. Similarly, Hou et al.^[46] identified that the use of iron and cobalt based MOFs into the polystyrene polymer can improve the flame retardancy by reducing the pHRR by 14% and 28% respectively. This improvement was attributed to the MOFs enhanced thermal barrier effect. Besides, the addition of MOFs into the thermoplastic polymer was explained by Evans et al.,^[47] where the ZIF-8 MOFs were homogeneously mixed with thermoplastic polyurethane and poly lactic acid at a very high weight loadings (50%). It was found that 3D printed sample of MOFs reinforced thermoplastic composites showed improved surface area and more importantly demonstrated the potential of utilizing these MOF reinforced thermoplastic composites as chemically active structures.

Although the hybrid fillers have the unique phenomenon of improving the mechanical and flame retardant properties of the thermoplastic composites, the influence of hybrid filler reinforced PA6 composites remains understudied. Hence, in this work, we fabricate various PA6 composites using waste GFs, GNPs and a water assisted

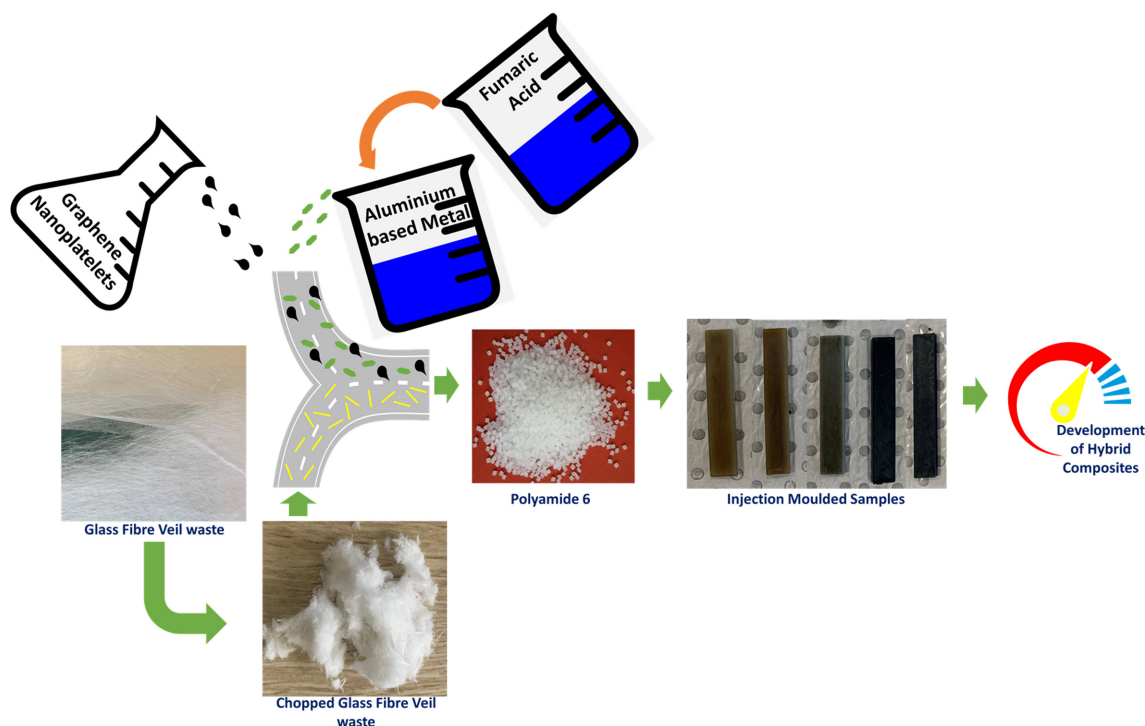


FIGURE 1 Experimental design to develop hybrid composites.

green aluminium metal organic framework (Al-MOF) through melt compounding evaluate their mechanical and flame retardant properties (Figure 1).

2 | EXPERIMENTAL

2.1 | Materials

Waste GF veils (GF) were provided by the local manufacturing suppliers Regina Fire Shield (Melbourne, Australia). PA6 (Zytel® 7301 NC010) was purchased from Goodfellow. Further XGNP-300 were purchased from XG Sciences. The purchased GNPs has an average diameter $<2 \mu\text{m}$, and contains a surface area of $\sim 300 \text{ m}^2/\text{g}$. The chemical reagents for the synthesis of Al-MOF are sodium hydroxide (NaOH), aluminium sulfate, fumaric acid which were purchased from Sigma Aldrich, Australia.

2.2 | Synthesis of Al-MOF

The synthesis of Al-MOF was performed by utilizing the sustainable methods where the pressure required to synthesize green MOF remained ambient. Initially, 66.6 g of aluminium sulfate was dissolved in 250 ml of deionized water (part A). Further, 23.2 g of fumaric acid and 20 g of NaOH was dissolved in another beaker with 250 ml of deionized water (part B). NaOH propagates reaction of

fumaric acid with water and therefore facilitates in dissolution. Once the clear solution is obtained, part B solution was slowly added into Part A under constant stirring at 90°C . Gradually, it was observed that the white precipitate formation takes place. After constant stirring for 1 h, the MOF solution was filtered and was washed with deionized water and ethanol. Finally, the synthesized material was dried at 80°C and was kept for activation at 120°C in the vacuum oven for over 12 h.

2.3 | Design of Experiments

2.3.1 | Utilization glass fibers

The waste GF veils washed with ethanol multiple times to remove any impurities and binders. it was then milled using the Pulverisette 19 cutting mill machine using the 6 mm mesh filter, and further these milled fibers were thoroughly washed again with ethanol to remove any remaining impurities. Fibers were dried in the oven at 70°C overnight.

2.3.2 | Modification of GF with GNPs and Al-MOF

The milled GF was mixed with GNPs and Al-MOF (different weight loadings, Table 1) using ethanol as solvent

| Samples | PA6 (wt%) | GF (wt%) | GNPs (wt%) | Al-MOF (wt%) |
|-------------------|-----------|----------|------------|--------------|
| PA6 | 100 | — | — | — |
| 20% GF | 80 | 20 | — | — |
| 30% GF | 70 | 30 | — | — |
| 20% GF/10% Al-MOF | 70 | 20 | — | 10 |
| 20% GF/10% GNPs | 70 | 20 | 10 | — |
| 20% GF/hybrid | 70 | 20 | 5 | 5 |

TABLE 1 The different weight loadings of GF, GNPs, and Al-MOF with PA6 as matrix.

at room temperature. After overnight stirring These solutions were filtered and then the resultant material was dried in oven at 70°C overnight.

2.3.3 | Composites fabrication

The samples were prepared by using the extrusion and injection molding techniques. Initially, different contents of GFs, GNPs, Al-MOF, and PA6 were fed into the extrusion. Before extrusion, all ingredients were dried at 60°C in a vacuum oven overnight. The compounding step was carried out by using Haake PolyLab (PTW16) including different temperature zones ranging from 230 to 240°C at 100 rpm. The extruded filaments were fully air dried and chopped into 2–3 mm granules which were further used in injection molding (Babyplast 6/12 Standard). Two different shot sizes including 30 and 45 mm were considered for preparation of tensile and flexural/DMA samples, respectively. The nozzle temperature was set to 260°C to avoid any blockages. The mold was set to be 70°C according to the technical datasheet recommendation.

2.4 | Measurements

GF tensile properties were measured using the Favimat + Robot 2 single fiber tester (Textechno H. Stein, Bavaria, Germany). The force–elongation data for individual fibers (at least 75 single fibers) loaded into a magazine were automatically recorded. Tensile load–elongation curves were obtained at a test speed of 2.0 mm/min using a gauge length of 25 mm and a pre-tension of 0.5 cN/tex according to ASTM D1577 linear density and ISO 11566 for fiber tensile test. Scanning electron microscopy (SEM) images were acquired on a Zeiss Supra 55VP at EHT voltage 5 kV, and Transmission electron microscope (TEM) images were captured using a Philips TEM at 300 kV in bright field mode. Brunauer–Emmett–Teller (BET) specific surface area was measured by a Micromeritics TriStar 3000 using adsorption

isotherm of nitrogen at 77 K was used to understand the surface area, pore size, and volume. The powder X-ray diffraction (XRD) measurements were performed by a PAN analytical X'Pert Pro Diffractometer (Cu K α radiation with $\lambda = 1.54184 \text{ \AA}$) in the range of 5–70° ($2\theta^\circ$), operating at 45 kV and 30 mA with a step size of 0.0525. Fourier transform infrared (FTIR) spectra were obtained by an FT-IR spectrophotometer of Bruker Optics using diamond as the background crystal. Malvern Mastersizer 2000 was employed to determine the particle sizes. Ethanol was used as a dispersion medium for particle size measurements. Thermogravimetric analysis (TGA) measurements were obtained by a Perkin–Elmer TGA instrument at 10°C/min heating rate under a nitrogen atmosphere with a flow of 60 ml/min. Differential scanning calorimetry (DSC) analyses were conducted by a TA Q200 DSC instrument from room temperature to 300°C at 10°C/min heating rate under a nitrogen atmosphere. The DSC scanning protocol was as follows: heating the sample from –10 to 300°C at 5°C/min, cool from 300 to –10°C at 5°C/min. Once the thermal history was erased and the residual stresses from injection molding were removed, the materials were heated again from –10 to 300°C at 5°C/min. Therefore, the data used for analysis was from the second heat cycle. For all the thermal characterizations, the samples weight was kept constant in the range of 15–18 mg. Further, the dynamic mechanical analysis (DMA) was performed using TA instrument. The double cantilever testing was performed on the reinforced thermoplastic composites. Temperature sweep was carried out the frequency range of 1 Hz in a temperature range of 20–130°C at a scanning rate of 2°C. In addition, the heat deflection temperature (HDT) was measured in accordance with ASTM D648. The measurements were taken at 1.82 MPa in a temperature range of 35–150°C with a scanning rate of 3°C. Further, mechanical properties of the reinforced thermoplastic composites were characterized through tensile and flexural testing methods on Instron Universal testing machine. Tensile tests were conducted using the ASTM D638 at a loading rate of 10 mm/min. A 30kN load cell was employed on both the flexural and tensile tests. Flexural tests were

TABLE 2 Comparison of mechanical properties of waste GFs used in this work with S-glass and E-glass fibers.

| Glass fiber properties (single fiber test) | Waste glass fiber veil | S-glass | E-glass | References |
|--|------------------------|---------|---------|------------|
| Tensile strength (GPa) | 0.80 | 4.89 | 3.45 | [49] |
| Tensile modulus (GPa) | 72.76 | 86.9 | 72.3 | [49] |
| Elongation (%) | 1.17 | 5.7 | 4.8 | [49] |
| Diameter (μm) | 12.11 | 8–16 | 6–17 | [50,51] |
| Cost (USD/kg) | 0.50 | 10 | 9 | [52] |

performed using the ASTM D790 at a strain rate of 1% /min. Pyrolysis Combustion Flow Calorimetry (PCFC), also known as microscale combustion calorimetry, has been shown to be a very valuable technique for screening flammability of different materials.^[48] This method also is an established ASTM standard for testing flammability characteristics of solid materials (ASTM D7309).

3 | RESULTS AND DISCUSSION

3.1 | Physical and structural characterization of hybrid fillers

The morphology of waste GF was examined using SEM and clean surface was observed after washing multiple times with ethanol and acetone (Figure S1A). To understand the inherent mechanical properties, 75 single filaments of waste GF were tested (Figure S1B). The average tensile strength obtained at 0.80 GPa, denoted significantly lower mechanical properties compared to the traditional S-glass or E-GFs (Table 2). But the modulus was observed at 72.76 GPa, hence, it can be inferred that the values remained approximately consistent with the traditional GFs. However, the elongation at break of waste GFs exhibited poor values at 1.17% and can be contributed to the manufacturing process of waste fibers. Given the fact that the properties of the waste GFs showed poor strength, it is expected that the resultant composites with PA6 will exhibit mechanical properties different to the traditional GFs. Figure (S1A,D) showcases that most waste GFs possess a length of <math> < 50 \mu\text{m}</math>.

In this work, MOFs were synthesized using water as the solvent, and consequently, the novel strategy of eliminating harmful chemicals such as dimethylformamide, tetrahydrofuran, and chloroform was accomplished. The as-synthesized Al-MOF was initially characterized by SEM and TEM analyses. It was inferred from the SEM images presented in Figure 2A, that the Al-MOF showcased an irregular shape across the spectrum with a particle size below 20 nm. Similarly, the SEM image of GNPs has been shown in Figure S2, where the agglomerated

particle of GNPs can be observed. The TEM imaging was also performed to confirm the formation of Al-MOF. Here, Figure S3A–F showcases the agglomerated Al-MOF containing C, O groups, and more importantly the presence of Al was also confirmed. Additionally, these Al-MOF and GNPs particles were measured to have a particle size distribution (Figure 3A) in the range of 0–40 μm .

The surface textural properties of the Al-MOF were analyzed using BET and the pore volume, and surface area was determined accordingly in Figure 3B,C. As observed, the adsorption/desorption curves showcased type IV isotherm (typical S shape) for both Al-MOF and GNPs.^[53] It can be further inferred that there is a narrow hysteresis curve between the adsorption and desorption phenomena. Incidentally, the isotherm observed is similar to the Al-MOF produced using DMF as a solvent.^[53] Also, the surface area observed was 843.48 m^2/g , indicating that improved surface area can be obtained by using water as a synthesis medium. Additionally, it needs to be asserted that a similar P/P0 trend was observed for GNPs (Figure 6B,C), for which the surface area was identified to be at 339.90 m^2/g .

The XRD peaks of Al-MOF are shown in Figure 2C. The diffracted peaks obtained for Al-MOF have presented the most prominent peaks at $2\theta = 10.2$ and 21.7° . These obtained peaks are in complete agreement with the literature for Al-MOF synthesized in organic solvents.^[53,54] Given that no additional secondary phases are obtained, it can be understood that the synthesized green Al-MOF has inherent robustness, that is, strong structural properties. Furthermore, the peaks acquired meet the miller indices at (111) and (311) ($2\theta = 10.2$ and 21.7°), respectively.^[55]

In this work, the FTIR peaks of the Al-MOF synthesized using green methods showcased peaks (Figure 2D) and is in correlation to the literature.^[55,56] Precisely, around 500 cm^{-1} , the Al-OH stretch is observed and at around 1600 cm^{-1} an O–H stretch can be identified. Furthermore, the TGA thermograms (Figure 4) of GF, GNPs, and Al-MOF were analyzed. The Al-MOF showcased the thermal stability over 400°C and is consistent with the

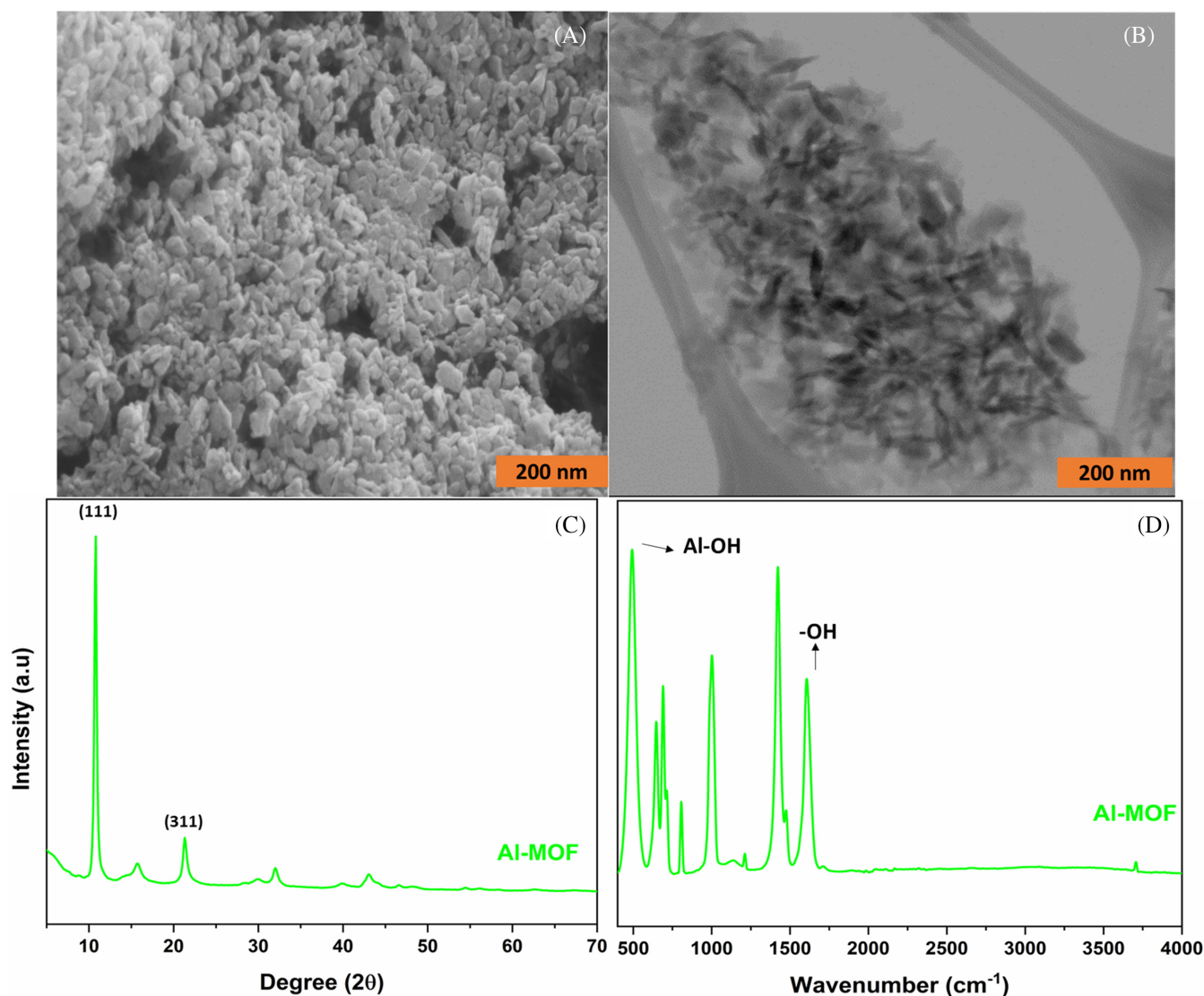


FIGURE 2 SEM (A), TEM (B), XRD (C), and FTIR (D) results of Al-MOF.

literature.^[56,57] It was observed that the char obtained at 700°C was around 43.1%, implying that the Al-MOF has the potential to exhibit flame suppression mechanism.^[58] Conversely, residue obtained for GF and GNPs were 92.8% and 89.6%, respectively.

3.2 | PA6 composites properties

3.2.1 | Structural properties of the PA6 composites

Figure 5A,B shows the DSC curves, upon cooling and heating of the composites in the temperature range of -10 to 300°C. The curves reported are obtained after removing the thermal history from the thermoplastic composites by heating the samples. For the development

of crystalline polymer reinforced thermoplastic composites, understanding the crystallinity and crystal behavior remains paramount.^[59] Therefore, evaluating the effect of filler reinforced PA6 composites will help in the understanding of reinforced thermoplastic composites thermal properties. PA6 composites traditionally contain two forms of crystals: α -form and γ -form.^[60] Here, in the current DSC study of PA6, α -rich form is identified at T_m of 221.4°C. Interestingly, all the melting temperature of filler reinforced composites, remains almost similar. This is primarily due to the unaltered crystal structure in the thermoplastic composites upon the addition of single or hybrid fillers. But 30% GF alongside PA6 showed higher T_m . This can be attributed to the increased weight loading of GF, and notably, the different thermal histories of GF and PA6. It was also inferred that, immediately after performing the slow cooling of the reinforced composites,

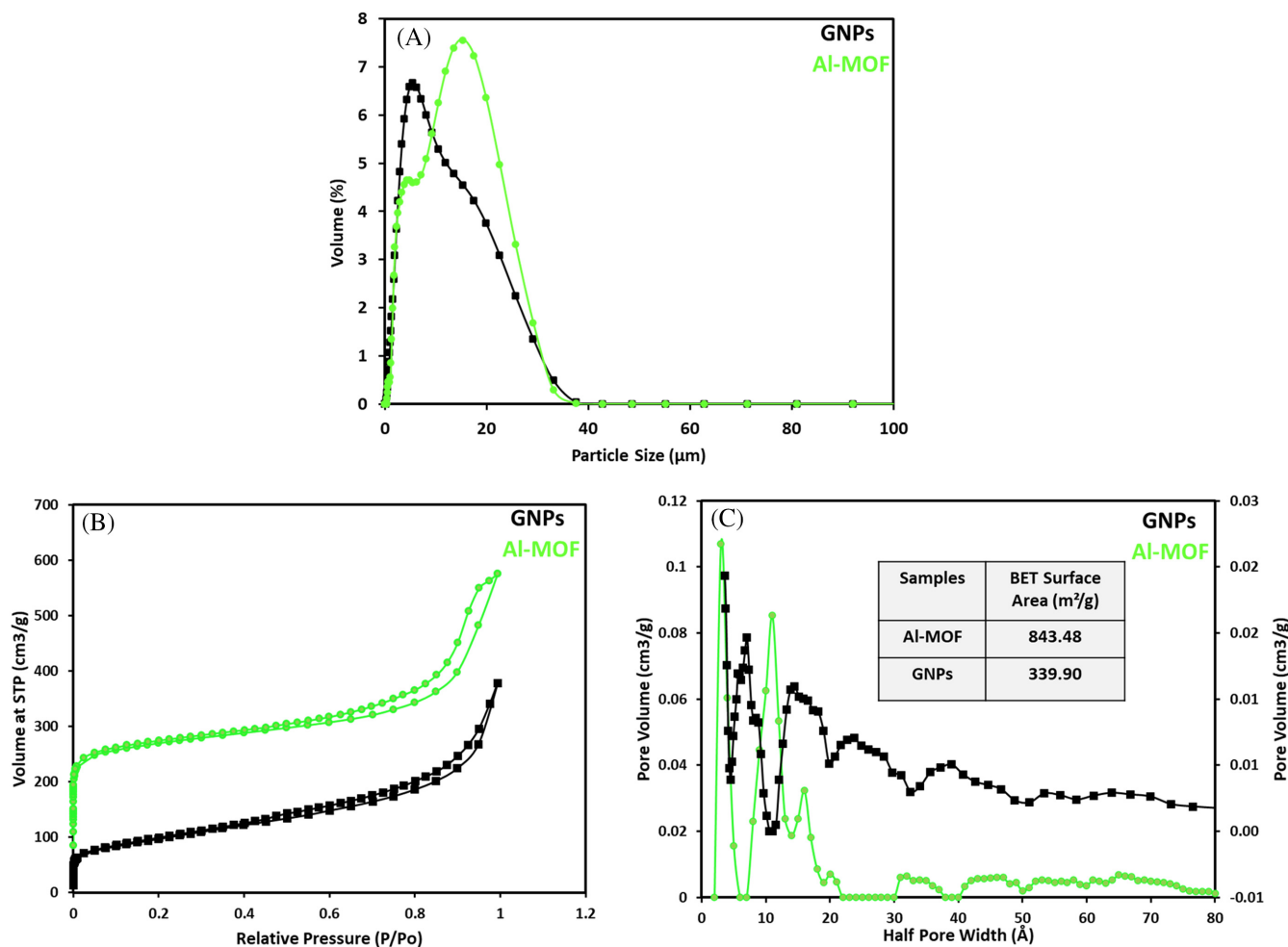


FIGURE 3 Particle size analyzer (A), BET analysis (B,C) of Al-MOF and GNPs.

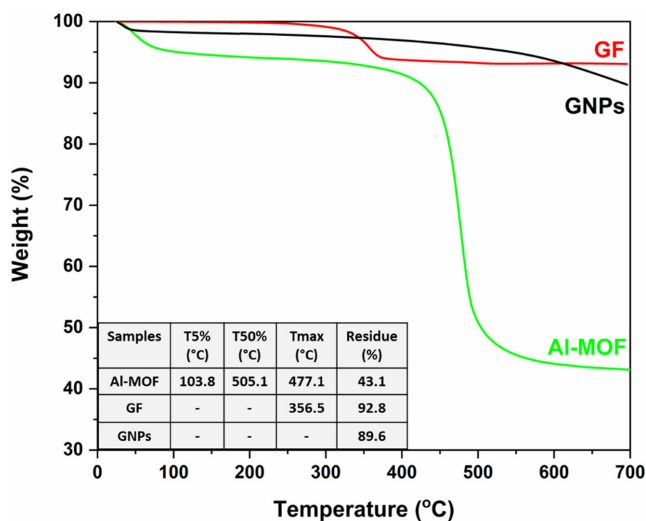


FIGURE 4 TGA of Al-MOF, GNPs, and GF.

the crystallization temperature (T_c) altered, resulting in the formation of thicker lamellar crystals, which are melted at higher values.^[61] Furthermore, the DSC

investigation exhibits the exothermic reaction of the thermoplastic composites during the stage of crystallization. It was observed that 10% addition of hybrid fillers and GNPs showcased the nucleating agent's effect in the PA6 composites. Table 3 exhibits the crystallization temperature (T_c) of these PA6 composites and showcases a positive shift to higher temperatures, compared to neat PA6 and other PA6 composites. Moreover, the improved nucleating reaction is the result of slow cooling process which allows crystals growth. In addition, the nucleating reaction starts at higher temperatures in the reinforced composites when compared to the pure PA6 composites. In this work, upon noticing the width of the crystallization peak (Figure 5B), the increasing width in the reinforced composites corresponds to the wider crystal size distribution of the PA6. Also, it was identified that the enthalpy of crystallization (ΔH_c) was decreasing for filler reinforced composites. This can be attributed to the increased polymer chain interaction which restricts polymer chain mobility, due to the increased addition of fillers.^[62] It can also be inferred from the curves that the

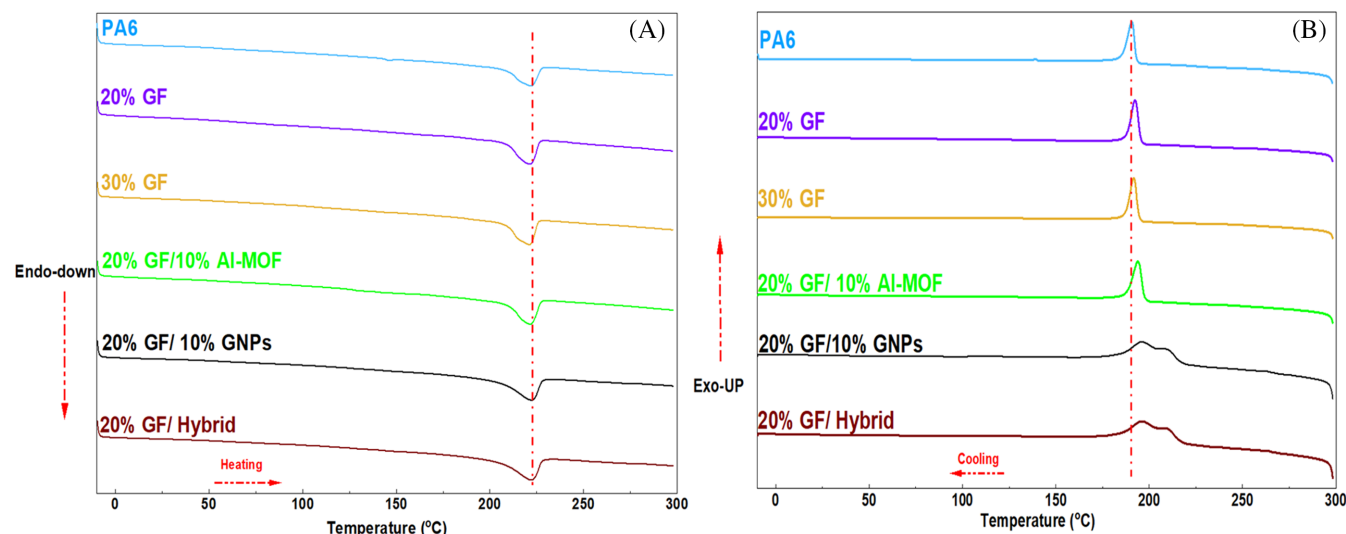


FIGURE 5 DSC curves heating (A) and cooling (B) of PA6 composites.

TABLE 3 Derived thermal characteristics obtained from DSC analyses showcasing T_c ($^{\circ}\text{C}$), T_m ($^{\circ}\text{C}$), ΔH_m (J/g), ΔH_c (J/g).

| Samples | PA6 | 20% GF | 30% GF | 20% GF/10% Al-MOF | 20% GF/10% GNPs | 20% GF/hybrid |
|------------------------------|-------|--------|--------|-------------------|--------------------------------|--------------------------------|
| T_c ($^{\circ}\text{C}$) | 190.7 | 192.4 | 191.7 | 194.1 | Peak 1: 197.1 Peak 2: 209.5 | Peak 1: 197.3 Peak 2: 208.4 |
| T_m ($^{\circ}\text{C}$) | 221.4 | 220.7 | 230 | 220.9 | 221.5 | 222.5 |
| ΔH_m (J/g) | 75.6 | 63.3 | 59.3 | 53.4 | 49 | 50.4 |
| ΔH_c (J/g) | 49.7 | 41.8 | 39.1 | 34.6 | 32.3 | 28.9 |

ΔH_m values clearly presents the decreasing trend upon increased weight loading of hybrid fillers. This asserts the fact that the addition of fillers disturbed the order in the crystalline phase of the pure PA6 composites.^[63] Hence the need to evaluate the crystallographic properties of the reinforced thermoplastics becomes paramount.

XRD of the hybrid filler reinforced PA6 composites are presented in the Figure 6. Traditionally, XRD is the most powerful tool to analyze the crystallization behavior of the composites. The diffraction peak for PA6 was identified at about 22.7° . This peak, as reported in literature, was found to be a γ crystalline form of PA6.^[64–66] The α -form diffraction peak ($2\theta = \sim 20^{\circ}$ ^[67]) observed is a very small shoulder peak and this can be attributed to the tested specimen's skin which would have dominated region of γ -form.^[66] Here, the addition of 20% GF and 30% GF did not showcase any peak shift, inferring that the addition of GF did not change the crystalline form of the reinforced PA6 composites. The similarity in the heights of peaks for PA6, 20% GF and 30% GF also showcases that the γ -form is the most dominated region and there is no clear peak for α -form in the 20% GF, 30% GF reinforced PA6 composites. The addition of 10% Al-MOF clearly, showcased a peak at around 10.2° which is the

characteristic peak for the Al-MOF,^[53] indicating the presence of Al-MOF in the 20% GF reinforced PA6 composites. GNPs was also confirmed when a sharp peak at 2θ was identified at around 27° , which is related to the GNPs (002) diffraction peak. Another peak at around 54.6° , the (004) diffraction peak was also observed^[68] in the GNPs sample. This XRD diffracted peaks was identified when 10% GNPs was added alongside 20% GF/PA6 and upon addition of 5% GNPs in hybrid composites. It was also observed that the intensities remained similar for both the composite structures. Also, the α -form and γ -form of PA6 was identified at 22.3° and 25° in both the composites. It needs to be elucidated that upon the addition of 10% GNPs, the α -form was identified to be weaker compared to the γ -form. This was due to the addition of increased weight loading of GNPs which weakens the α -form.^[69] However, at 5% weight loading of GNPs in hybrid composites the α -form was improved. Moreover, it was also identified in the hybrid composite that, in addition to the GNPs, presence of Al-MOF was also identified at 10.2° . Nonetheless, compared to the 20% GF/10% Al-MOF composites, the peak intensity can be identified to be reduced. This can be attributed to the reduced weight loading of Al-MOF.

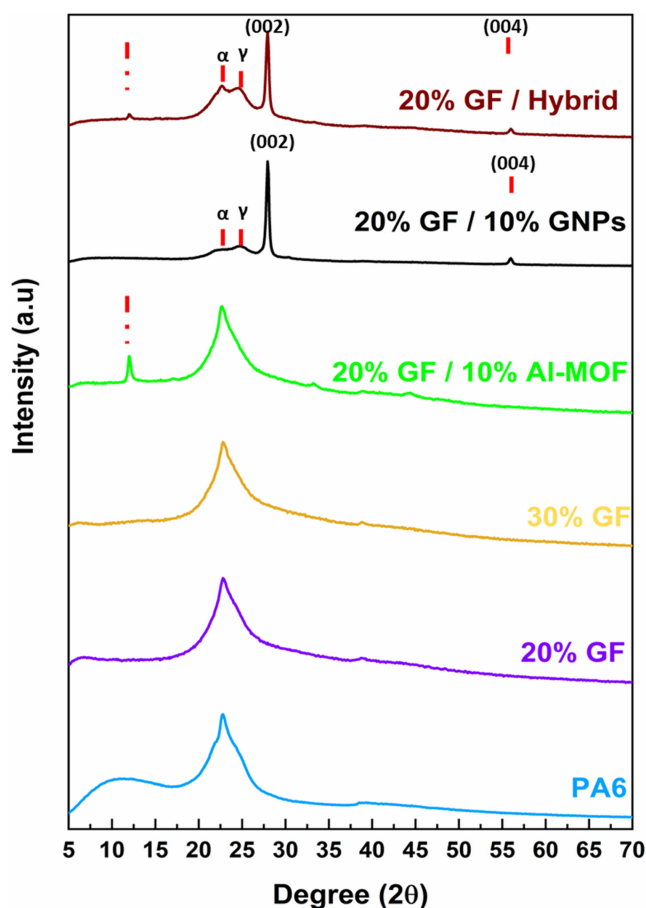


FIGURE 6 XRD peaks of the filler reinforced PA6 composites.

3.2.2 | DMA properties of the PA6 composites

DMA is traditionally used to determine the mechanical damping and the stiffness of the composites as a function of time, frequency and temperature.^[70] The storage modulus, $\tan \delta$ and the T_g of the composites have been studied accordingly to understand the viscoelastic materials properties. The T_g of composites samples can be interpreted from the curves to evaluate the cross linking mechanism of the filler alongside polymer. Furthermore, the intensity of the $\tan \delta$ peaks helps in understanding the materials inherent property of being elastic and non-elastic behavior.

In this study, it is evident that the addition of fillers develops a positive reinforcement mechanism and therefore exhibits improvement in the storage modulus of the composites. The values interpreted from the DMA curves (Figure 7A,B) are illustrated in Table 4. The addition of 20% GF and 30% GF showed storage modulus improvement by 90.1% and 126.8% respectively when compared to the neat PA6 composites, clearly indicating the presence of GF with high modulus in the PA6 matrix. It is

also promising to identify that although the modulus was improved upon addition of 10% Al-MOF (+127%) with respect to the neat PA6, improvement of storage modulus in 10% Al-MOF composites was not significant when compared to the 30% GF reinforced composites. But, the addition of 10% GNPs nanofillers improved the modulus significantly (+167%) and, the hybrid filler also showcased a significant improvement (+180%) in the storage modulus property when compared to neat PA6 composites. Also, the improvement in 10% addition of hybrid filler is 4.7% and 22.9% upon comparison with the 10% GNPs and 10% Al-MOF.

Figure 7B showcases that the $\tan \delta$ peak values decrease with the increasing addition of the nanofillers. It is implied that the $\tan \delta$'s magnitude depends directly on the nature of the polymeric systems and hence the values signify the energy dissipation as a result of molecular motions and friction.^[71] Therefore, it can be inferred that the decreasing $\tan \delta$ peak is the result of the restricted polymer chain movement due to the presence of reinforcing agents.

The T_g values was inferred from the $\tan \delta$ peaks of the thermoplastic composites. It was observed that the addition of reinforcement fillers leads to the improvement in the T_g of the composites. Since the addition of fillers potentially increases the cohesive energy density in the system and hence the positive reinforcement is identified. This cohesive energy density^[72] can be considered as the physical quantity to evaluate the intermolecular forces upon addition of fillers in the matrix. To elaborate the behavior of T_g upon addition of fillers, the works conducted by Tsagaropoulos et al.^[73] and Zhang et al.^[74] assist in evaluating the interactions between the polymer chains and the nanoparticles. It can also be inferred that the addition of fillers hinders the motion of the PA6's molecular chain, which potentially occurs due to the entanglements and the improved interfacial interactions. However, it is noted that the shift in T_g is not significant upon addition of Al-MOF and GNPs in hybrid nanofillers and that the T_g of 10% hybrid composites is significantly higher than the pure PA6 composites. The improvement of 27°C can be attributed to the enhanced synergistic effect of Al-MOF alongside GNPs, furthermore, the higher weight loadings of the fillers (10% Hybrid and 20% GF) in the PA6 matrix may have also contributed toward the improved T_g .

Finally, the DMA testings were performed to obtain HDT values of neat and reinforced PA6 composites. HDT is used to predict the polymeric materials ability to withstand at higher temperature. Primarily, it has been identified that the HDT for the pure PA6 is about 45.4°C. As expected, upon reinforcing the PA6 composites with fillers, the HDT values increased significantly by 85% and

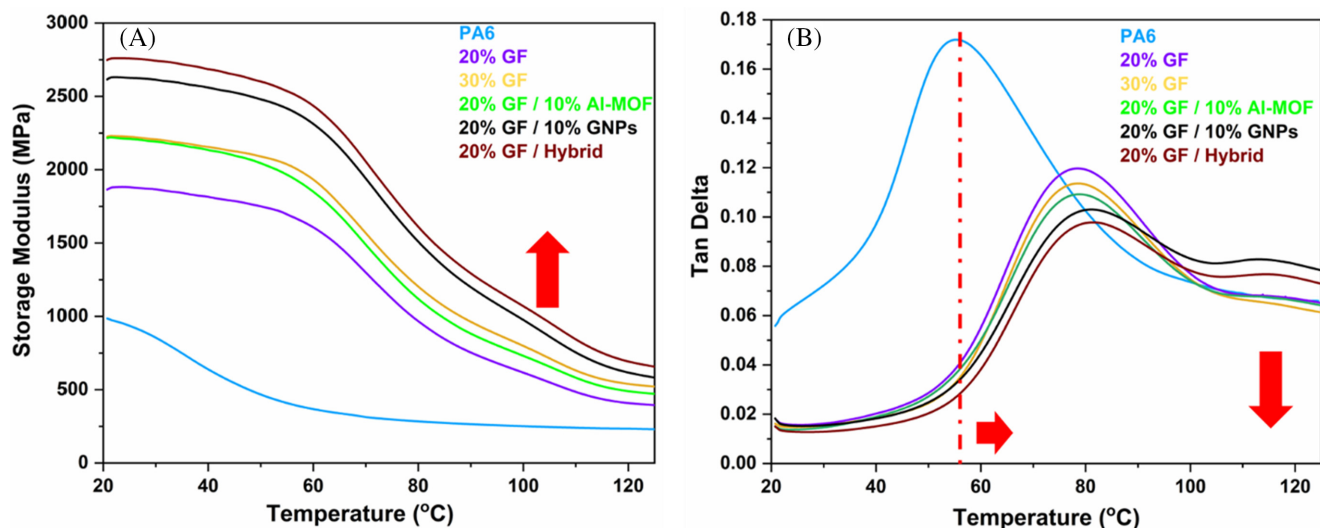


FIGURE 7 Storage modulus (A) and $\tan \delta$ (B) of PA6 composites.

TABLE 4 Storage modulus, $\tan \delta$, T_g , and HDT data derived from DMA curves.

| Samples | PA6 | 20% GF | 30% GF | 20% GF/10% GNPs | 20% GF/10% Al-MOF | 20% GF/hybrid |
|-----------------------|------|--------|--------|-----------------|-------------------|---------------|
| Storage Modulus (MPa) | 981 | 1864 | 2225 | 2623 | 2234 | 2747 |
| T_g (°C) | 55.3 | 78.2 | 78.8 | 79.7 | 80.0 | 82.4 |
| HDT @ 1.82 MPa | 45.4 | 84.1 | 95.9 | 99.1 | 94.4 | 100.4 |

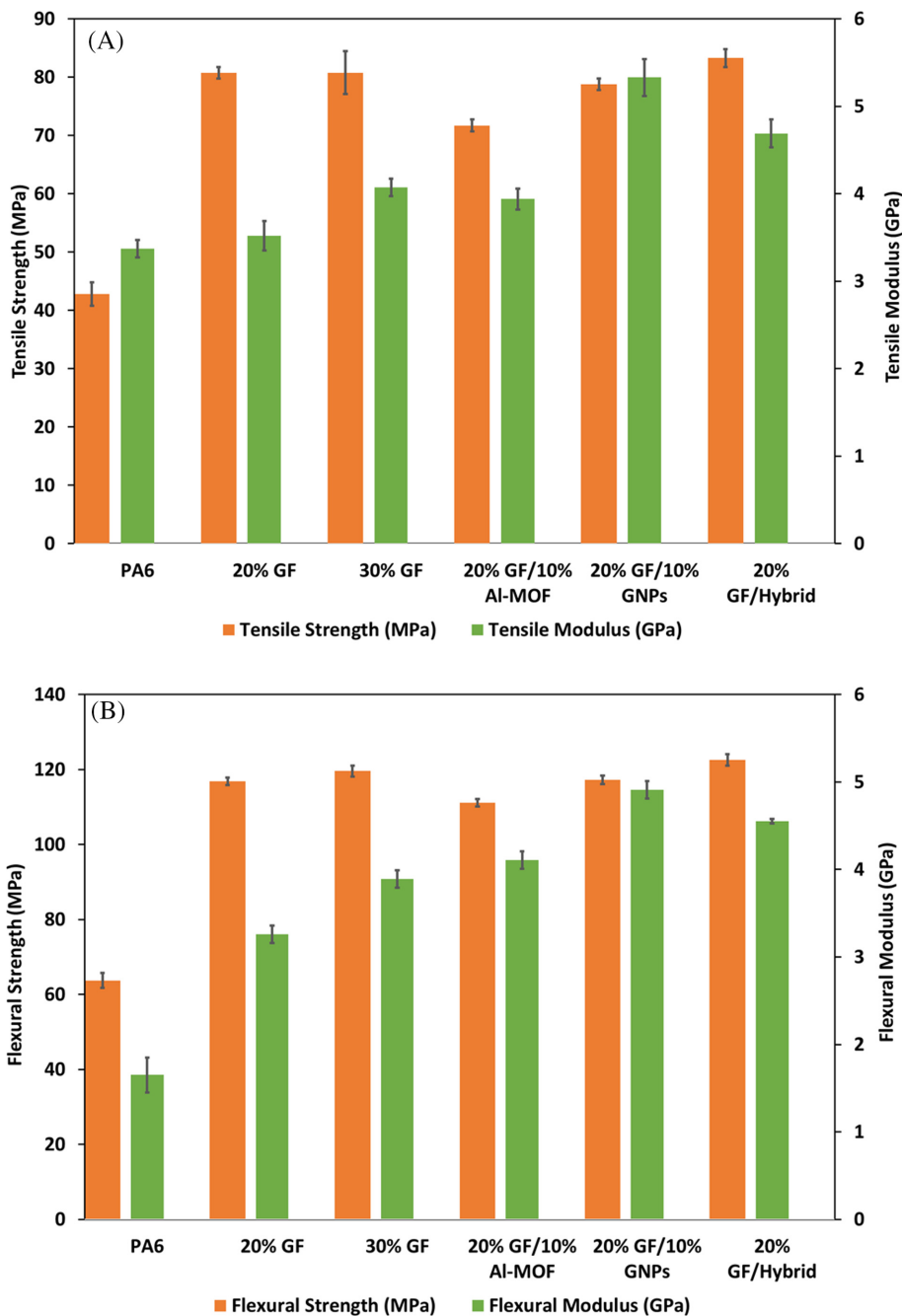
111% for 20% GF, 30% GF, respectively, compared to the neat PA6. It was observed that the addition of 10% GNPs improved the HDT values to 99.1°C, however, when compared to the 10% Al-MOF reinforced thermoplastics, they exhibited decreasing HDT by 4.7%. This drop in the HDT values can be ascribed to the plasticizing effect of Al-MOF at higher temperatures. The 10% hybrid filler showcased superior properties compared to all the reinforced samples. Also, it can be concluded from the HDT values of the reinforced composites that improved dispersion, interfacial interaction, and the change in the crystal regions, significantly affects the HDT of the reinforced composites.^[75]

3.2.3 | Mechanical properties of the PA6 composites

The tensile and flexural testings of PA6 and its composites were performed, and their results are illustrated in Figure 8A,B. Initially, it was observed that the pure PA6 composites has a tensile and flexural strength of 42.8 and 63.7 MPa, respectively. As expected, the addition of 20% GF led to 88% increase in tensile strength, but the strength for the 30% GF remained almost similar. This can be attributed to the agglomeration of the GF in the

PA6 reinforced composites. Also, the incorporation of 10% Al-MOF, 10% GNPs into 20% GF/PA6 composite decreases the tensile (11.2%, 2.4%) and flexural (7.1%, 2%) strength, respectively, when compared to the 30% GF/PA6 composite. This decrease in properties for Al-MOF can be attributed to the plasticizing effect of nanofillers in the matrix and agglomeration due to increased weight loading.^[76] Similarly, the increased weight loading of GNPs traditionally leads to the decrease in mechanical properties because of agglomeration.^[77] As identified from the mechanical properties of the thermoplastic composites, the incorporation of 10% hybrid fillers (5% Al-MOF and 5% GNPs) into 20% GF/PA6 composite improved the tensile and flexural strength by 94.5% and 92.3% respectively when compared to pure PA6 composites. Interestingly, in comparison to the 30% GF, the 10% hybrid fillers performed slightly better. Although negligible, however this marginal improvement of flexural (+3.1%) and tensile (+2.4%) strength can be attributed to the enhanced synergistic effect of Al-MOF alongside GNPs in the 20% GF. Although reinforcing increased weight loading of Al-MOF has plasticizing effect, yet the improved interfacial interaction with GNPs in the hybrid filler leading to the improved synergistic effect can be attributed to the carboxylic functional group in Al-MOF. Additionally, it needs to be highlighted that

FIGURE 8 Tensile (A); and flexural (B) properties of reinforced composites.



the addition of 10% hybrid fillers improved the tensile and flexural modulus by 39.1% and 175.7%, respectively, when compared to the pure PA6 composites.

Mechanisms behind these mechanical improvements were investigated using SEM observations on fracture surface of composites. Fracture surface morphology from Figure 9 (a-l), clearly showcases neat and clean surface for the pure PA6 thermoplastics. Here, the reinforced PA6 composites exhibited rough surface morphologies. The addition of 20% GF and 30% GF into PA6 resulted in a ductile fracture in the composites. It was also observed that the GF/PA6 composites generally presented weak interfacial interaction, inferring from the presence of

holes/voids in the Figure 9B,C. These voids can be attributed to the fiber pull due to the weak interfacial interaction. Moreover, pultruded fibers can also be seen in the fracture morphology with increasing GF content (Figure 9C). This weak interfacial interaction can also be related to the absence of compatibilizer the short GF, potentially developing positive reinforcing mechanism leading to the improvement in the mechanical properties of the reinforced composites when compared to the neat PA6 composites. Interestingly, the addition of 10% GNPs into 20% GF/PA6 composite exhibited a brittle nature (Figure 9H,I). Improved dispersion and distribution of GNPs into the 20% GF/PA6 composite was observed and

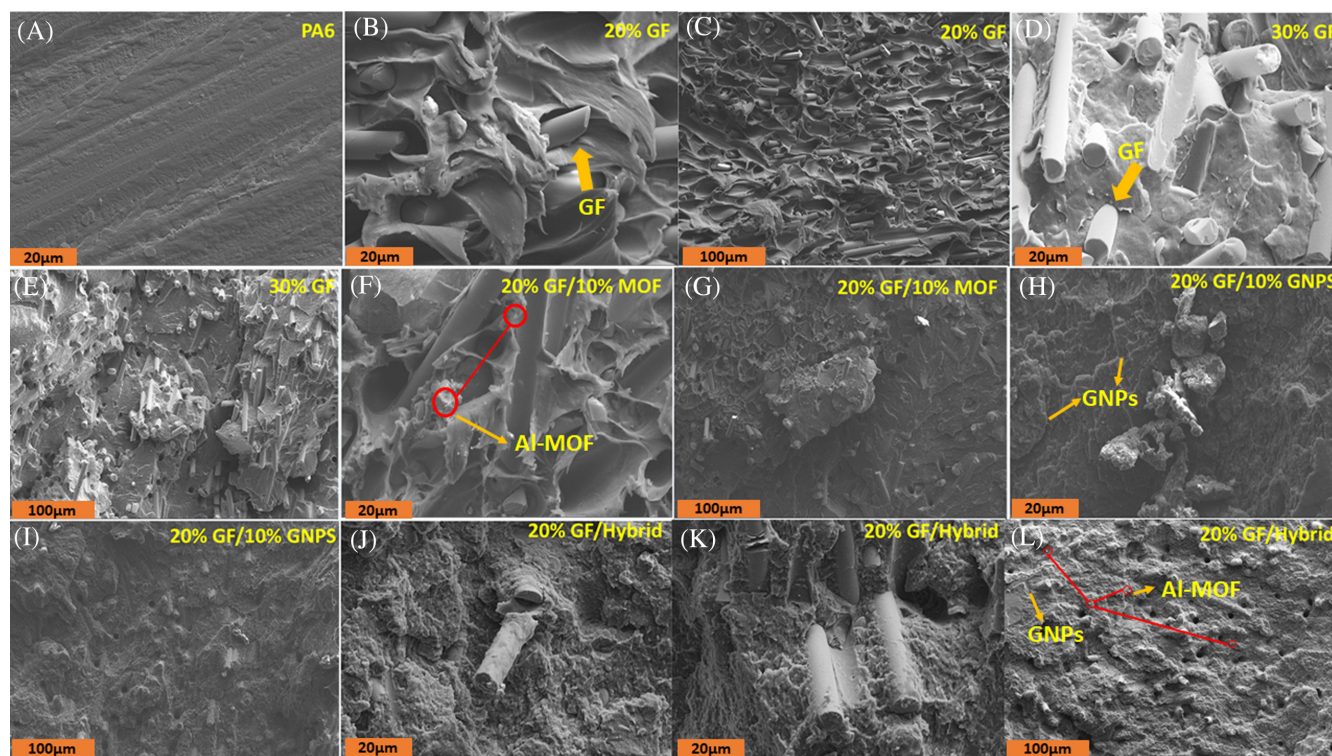


FIGURE 9 Fracture study of reinforced PA6 composites (A) neat PA6; (B,C) 20% GF; (D,E) 30% GF; (F,G) 20%GF/10%Al-MOF; (H,I) 20%GF/10%GNPs;(J–L) 20%GF/hybrid.

that the GNPs exhibited very minimal agglomeration. Here, the interfacial interaction between the GF and PA6 matrix improved with minimal voids observed from the fiber pull out test. It is assumed that the GNPs formed a network like connection in the PA6 matrix with extremely rough patches observed throughout. Hence, these features can be ascribed to improvement in the mechanical properties when compared to the pure PA6 reinforced composites. However, due to the increased agglomeration, these GNPs reinforced thermoplastic composites, showed decreased mechanical properties when compared to the 20% or 30% GF reinforced composites. Similarly, it can be observed from the Figure 9F, G, that the Al-MOF (10% wt loading) when reinforced alongside 20% GF/PA6 composite demonstrated a decreasing trend when compared to the 20% and 30% GF composites. This can be attributed to the plasticizing effect of Al-MOF, furthermore, the porous nature of Al-MOF, leads to poor interfacial interaction between the Al-MOF and polymer. This eventually results in the poor fiber/Al-MOF interaction demonstrated in decreased mechanical properties of the final composites. Although, agglomeration phenomenon can be identified in various nanofillers, nonetheless, in this work the introduction of 10% Al-MOF alongside 10% GNPs and 20% GF, showed a positive trend in the mechanical properties and fracture mechanisms. In Figure 9J,K,L, the improved fiber-matrix

interfacial interaction can be observed alongside GNPs and Al-MOF nanofillers. This improvement can be ascribed to the improved crack propagation phenomenon. Al-MOF has inherently lower dimensional stability compared to the graphene. However, due to the having carboxylic groups, the Al-MOF provides better interfacial interactions and compatibility with PA6. The possible Al-MOF interaction is hydrogen bonding of carboxylic groups with the amide bonds of PA6 chains. Based on the mechanical results shown in Figure 8, although there is the same filler content in 20% GF/10% Al-MOF, 20% GF/10% GNPs, and 20% GF/10% hybrid PA6 composites, the PA6 composite containing hybrid filler demonstrates higher mechanical properties. Therefore, there is a synergistic effect in reinforcement of PA6 composites using Al-MOF and GNPs. Since Al-MOF has better interfacial interactions with PA6 chains, they can act as a bridge between GNPs and PA6 chain to improve the compatibility of GNPs with PA6.

3.2.4 | Thermal stability and fire retardancy of the PA6 composites

Figure 10 showcases the overlay of TGA curves of PA6 and the filler reinforced composites. The degradation temperature at 5% weight loss ($T_{5\%}$), temperature at

weight loss of 50% ($T_{50\%}$), temperature at maximum rate of degradation (T_{max}), and residue (%) values have been identified and presented in Table 5. It can be observed that the pure PA6 composite exhibits $T_{5\%}$ at 360°C. The $T_{5\%}$ was enhanced by 22, 30, and 21°C upon addition of 10% Al-MOF, 10% GNPs and 10% hybrid fillers, respectively, alongside 20% GF. Also, the T_{max} occurred at 447°C for pure PA6, but, the addition of GF and nanofillers resulted in a decreasing trend in the T_{max} . The TGA analyses of the samples presented an improvement in the $T_{50\%}$ when the addition of 10% GNPs and 10 hybrid filler into 20% GF/PA6 composite. Nonetheless, the influence of 10% hybrid fillers in 20% GF/PA6 composite showed improvement at $T_{50\%}$, the degradation temperature was identified to be less than the 10% GNPs reinforced 20% GF/PA6 composite. This can be attributed to the presence of Al-MOF inside the 10% hybrid nanofillers which can be degraded in lower temperatures. Effectively, the same trend was identified when 10% Al-MOF was added to the 20% GF/PA6 composites, where the reduction in T_{max} and $T_{50\%}$ with respect to the pure PA6 was observed. Accordingly, this trend is in correlation with the literature where the addition of MOFs^[78] into thermoplastic

polymers tends to decrease the thermal degradation properties. However, the addition of GNPs^[79] supports the effective degradation of the composites. Furthermore, to understand the performance of the PCFC testing technique, residue analysis was also performed. As expected, it was observed that the pure PA6 shows poor residue and therefore the pure PA6 will most likely exhibit poor flame retardancy. However, addition of the GF, GNPs and Al-MOF led to improved residual properties (Table 5). Hence, understanding the effect of the residue and the impact of nanofillers on the flame retardancy of the thermoplastic composites remains important.

Furthermore, LOI can be calculated using the TGA results and in this work the LOI is estimated from the van Krevelen's equation^[80]:

$$LOI = 17.5 + 0.4Y \quad (1)$$

where Y is the char yield at 500°C.

The LOI analysis of the reinforced composites as showcased in Table 5, exhibits improvement in the flame retardancy of the composites when waste GF and nanofillers such as GNPs and Al-MOF were reinforced with PA6

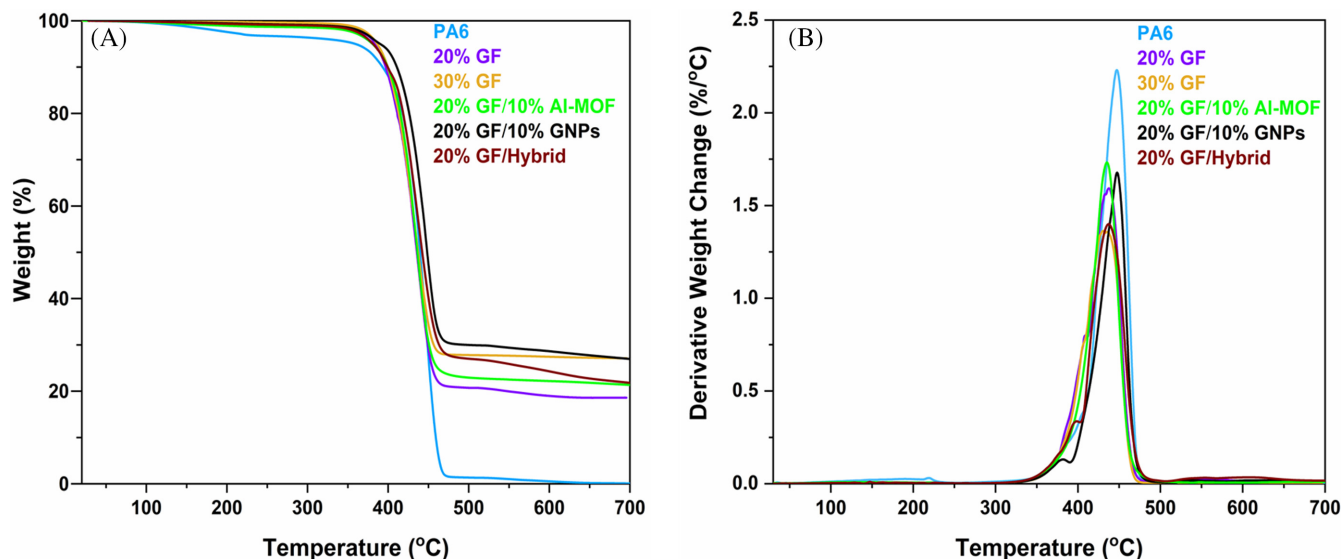


FIGURE 10 TGA (A) and DTG (B) curves of the various PA6 composites.

TABLE 5 Data derived from TGA curves.

| Samples | PA6 | 20% GF | 30% GF | 20% GF/10% Al-MOF | 20% GF/10% GNPs | 20% GF/hybrid |
|-----------------|------|--------|--------|-------------------|-----------------|---------------|
| $T_{5\%}$ (°C) | 360 | 384 | 386 | 382 | 390 | 381 |
| $T_{50\%}$ (°C) | 439 | 435 | 436 | 436 | 448 | 442 |
| T_{max} (°C) | 447 | 436 | 432 | 434 | 447 | 436 |
| Residue (%) | 0.08 | 18.6 | 27.1 | 21.3 | 26.9 | 21.8 |
| LOI (%) | 17.5 | 24.9 | 28.3 | 26.1 | 28.2 | 26.2 |

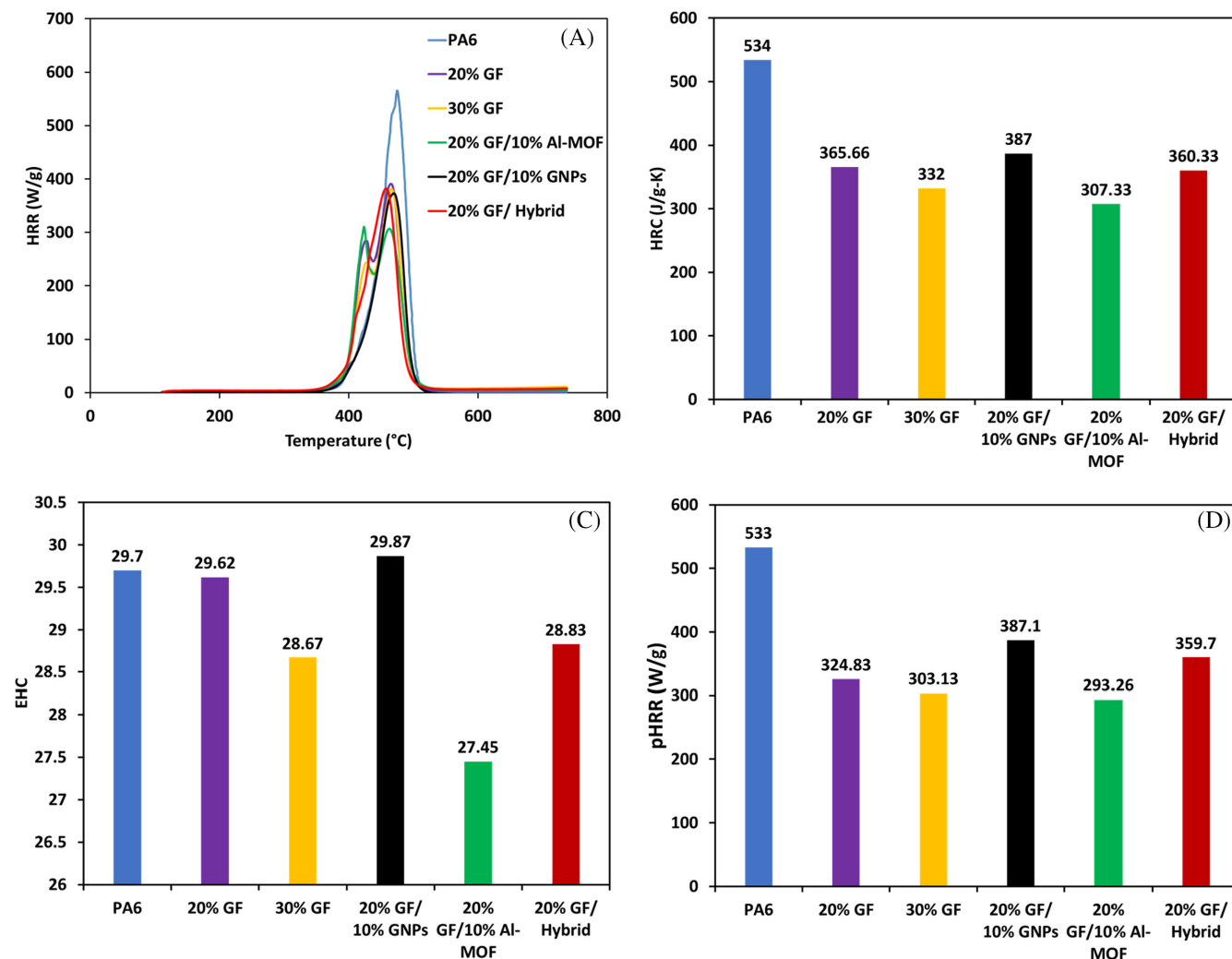


FIGURE 11 PCFC results of PA6 composites HRR (A), HRC (B), EHC (C), and pHRR (D).

thermoplastic composites. It can be observed that the addition of 10% hybrid filler clearly improves the LOI from 17.5% to 26.2%.

Similarly, the addition of 20% GF (24.9%) and 30% GF (28.3%) also exhibited improvements when compared to the neat PA6 composites LOI value of 17.5%. This improvement in the LOI can be attributed to the synergistic effects of the nanofillers in the PA6 matrix, which potentially acts as the barrier to suppressing the flame growth. Furthermore, it was found that there is a linear relationship between the LOI, heat release rate (HRR) and peak heat release rate (pHRR) values.^[81] Hence, to understand the flame retardant properties of the reinforced filler in comparison to the pure PA6 composites, PCFC testing was performed.

Figure 11A–D shows the results of PCFC testing of the pure PA6 and their various composites. The properties obtained are pHRR, HRR, effective heat of combustion (EHC), heat release capacity (HRC), total peak heat

release rate (TpHRR), total heat release rate (THR) and the char residue. HRC and pHRR are the important parameters in the identification of flame retardant properties.^[48,82,83] HRC is traditionally defined as the ratio between the maximum heat release rate and the constant heating rate. Additionally, the pHRR is defined as the intensity of the flame growth. It is significant to understand that neat PA6 reacts poorly with respect to the flame, showcasing HRC and pHRR values of 534 (J/g k), 533 (W/g). However, it can be inferred that the addition of GF (20% and 30%) reduces the HRC values significantly by 31.5% and 37.8%, respectively. Similarly, the pHRR values decreased by 39% (20% GF) and 43.1% (30% GF). These decreased properties are due to the increasing char residue formation upon the addition of GF.^[84–86]

The addition of 10% Al-MOF resulted in improved properties among all the reinforced PA6 composites and therefore asserting the influence of MOFs on flame retardant applications. This is in line with previous reports

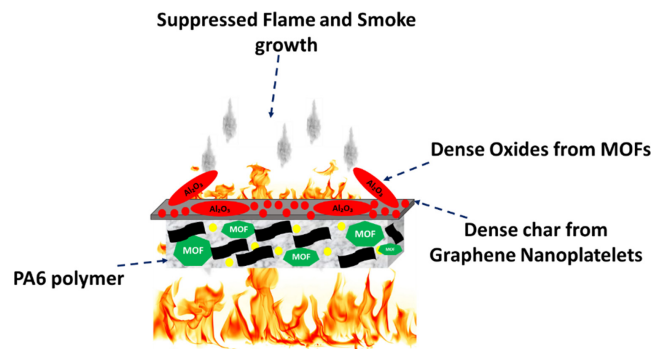


FIGURE 12 Flame retardancy mechanism of GNPs/Al-MOF reinforced 20% GF/PA6 composites.

that the addition of MOFs creates a barrier effect in the composites, leading to improvement in the flame retardant properties (Figure S4). The Al-MOF decomposes when exposed to fire and forms layers of metal oxides, which therefore delays the fire propagation of the composites. The development of the char layer caused the formation of metal oxides of Al-MOF during the flame growth led to the decrease in HRR, HRC, EHC and the pHRR values of the 10% Al-MOF/ 20% GF composites. Also, the inclusion of 10% hybrid fillers showed improved composite flame retardancy when compared to the neat PA6.

Based on the thermal and flame retardant behaviors, it can be concluded that the addition of Al-MOF improves the thermal stability and reduces the flammability of the Al-MOF reinforced thermoplastic composites. The proposed mechanism is presented in Figure 12, which exhibits the effect of hybrid fillers when reinforced with 20% GF/PA6 composite. Due to the Al-MOF presence, the oxides of aluminium at higher temperatures form a dense layer and therefore, suppress the flame growth. Additionally, the presence of GNPs significantly improves the char formation and therefore, restricts the flow of harmful gases during the flame extinguishing mechanisms. This combined reaction of restricting the flame growth and suppressing the harmful gases by utilizing the improved char formation, ensures superior flame retardancy when compared to neat PA6 composites. Although the flame retardancy of the pure Al-MOF reinforced 20% GF/PA6 composites are better than the other compositions, utilizing hybrid GNPs and Al-MOF can lead toward development of novel composite structures with improved mechanical and fire retardancy properties.

4 | CONCLUSIONS

In this work, an Al-based MOF was synthesized by using water as solvent and further utilized to develop

multifunctional PA6 thermoplastic composites by hybridizing with GNPs and waste GF. Initially, the effect of hybrid fillers on PA6 matrix was studied using DSC and consequently, the crystalline characteristics was analyzed utilizing XRD. Later, the thermomechanical and mechanical properties of the reinforced thermoplastic composites were evaluated. It was observed that the as developed 10% hybrid filler reinforced composite structure including industry grade 5% GNPs and 5% Al-MOF exhibited improved mechanical and flame retardant properties when compared to the neat PA6 composites. Also, the addition of 10% hybrid filler/20% GF in PA6 matrix showed 94% and 39% improvement in tensile strength and modulus, respectively. Similar trend was observed in the flexural properties where addition of 10% hybrid filler/20% GF resulted in improvement of strength and modulus by 92.3%, 175.7%, respectively. These enhanced mechanical properties of the reinforced thermoplastic composites can be attributed to the synergistic effects of GNPs and Al-MOF nanofillers alongside waste GF in the PA6 matrix. It was found that the addition of 10% hybrid fillers (5% GNPs, 5% Al-MOF) into the 20% GF-PA6 composites led to 4.8% and 3.1% improvements in flexural and tensile strengths respectively. Although minimal, identical trend was observed upon addition of 30% GF, which exhibited increase of flexural and tensile strength by 2.4%, 3.10%, respectively. Here, it needs to be asserted that the improvements observed is due to the mere addition of 5% nanofillers (Al-MOF and GNPs each) highlighting the synergistic effect of nanofillers on performance improvement of PA6. The synergistic effect is particularly highlighted in the case of GNPs and Al-MOF in improving the flame retardant properties. Addition of 10% this hybrid filler led to decreased HRR (37.5%), HRC (32.5%) and pHRR (32.5%) when compared to neat PA6 thermoplastic composites. Additionally, the UL-94 testing, clearly showed the enhanced effect of GNPs and Al-MOF in the hybrid fillers. Here, UL-94 of 10% hybrid fillers reinforced composites passed V2 rating (i.e., dripping, without flame) while PA6 composites showed no rating, that is, dripping with flame.

This study demonstrates the potential of MOF/graphene hybrid fillers in development of multifunctional thermoplastic composites using recycled materials and sustainable synthesis approaches, thus creating a pathway for advance development of reinforced thermoplastic composites for applications in automotive and beyond.

ACKNOWLEDGMENTS

The authors would like to thank Deakin University's Advanced Characterization team for the use of Electron microscopy facility. This research was supported by the

Australian Research Council Training Centre for Light Weight Automotive Structures (ATLAS) - IC160100032. Open access publishing facilitated by Deakin University, as part of the Wiley - Deakin University agreement via the Council of Australian University Librarians.

DATA AVAILABILITY STATEMENT

The raw/processed data required to reproduce these findings cannot be shared at this time as the data also form part of an ongoing study.

ORCID

Minoo Naebe  <https://orcid.org/0000-0002-0607-6327>

REFERENCES

- [1] E. Araujo, E. Hage, A. Carvalho, *J. Mater. Sci.* **2004**, 39(4), 1173.
- [2] C. Zhao, G. Hu, R. Justice, D. W. Schaefer, S. Zhang, M. Yang, C. C. Han, *Polymer* **2005**, 46(14), 5125.
- [3] S. Yuan, F. Shen, C. K. Chua, K. Zhou, *Prog. Polym. Sci.* **2019**, 91, 141.
- [4] D. Barfuss, C. Garthaus, M. Gude, R. Grützner, *Int. J. Autom. Compos.* **2016**, 2(3–4), 299.
- [5] R. Stewart, *J. Reinfor. Plast.* **2010**, 54(2), 22.
- [6] A. El-Sabbagh, L. Steuernagel, G. Ziegmann, D. Meiners, O. Toepfer, *Composites, Part B* **2014**, 62, 12.
- [7] K. Tanaka, S. Mizuno, H. Honda, T. Katayama, S. Enoki, *J. Solid Mechan. Mater. Eng.* **2013**, 7(5), 520.
- [8] G. Dlubek, F. Redmann, R. Krause-Rehberg, *J. Appl. Polym. Sci.* **2002**, 84(2), 244.
- [9] G. Srinath, R. Gnanamoorthy, *Compos. Sci. Technol.* **2007**, 67(3–4), 399.
- [10] P. Hornsby, J. Tung, K. Tarverdi, *J. Appl. Polym. Sci.* **1994**, 53(7), 891.
- [11] A. Güllü, A. Özdemir, E. Özdemir, *Mater. Des.* **2006**, 27(4), 316.
- [12] P. Curtis, M. Bader, J. Bailey, *J. Mater. Sci.* **1978**, 13(2), 377.
- [13] O. Zabihi, M. Ahmadi, C. Liu, R. Mahmoodi, Q. Li, R. M. Ghandehari Ferdowsi, M. Naebe, *Sustainability* **2020**, 12(2), 641.
- [14] J. Chen, K. Fu, Y. Li, *Compos. A Appl. Sci. Manuf.* **2021**, 140, 106160.
- [15] E. Vázquez-Núñez, A. M. Avecilla-Ramírez, B. Vergara-Porras, M. López-Cuellar, *Polym. Compos.* **2021**, 29, 09673911211009372.
- [16] B. P. Chang, A. Rodriguez-Urbe, A. K. Mohanty, M. Misra, *Renew. Sustain. Energy Rev.* **2021**, 152, 111666.
- [17] M. Sharma, R. Sharma, S. C. Sharma, *Mater. Today: Proc.* **2021**, 46, 6482.
- [18] S.-Y. Lu, I. Hamerton, *Prog. Polym. Sci.* **2002**, 27(8), 1661.
- [19] O. Zabihi, M. Ahmadi, Q. Li, M. R. G. Ferdowsi, R. Mahmoodi, E. N. Kalali, D.-Y. Wang, M. Naebe, *J. Clean. Prod.* **2020**, 247, 119150.
- [20] O. Zabihi, M. Ahmadi, R. Yadav, R. Mahmoodi, E. Naderi Kalali, S. Nikafshar, M. R. Ghandehari Ferdowsi, D.-Y. Wang, M. Naebe, *ACS Sustainable Chem. Eng.* **2021**, 9(12), 4463.
- [21] D. G. Papageorgiou, I. A. Kinloch, R. J. J. C. Young, *Carbon* **2015**, 95, 460.
- [22] O. Zabihi, M. Ahmadi, T. Abdollahi, S. Nikafshar, M. Naebe, *Sci. Rep.* **2017**, 7(1), 3560.
- [23] O. Zabihi, M. Ahmadi, Q. Li, S. M. Fakhrohoseini, Z. Komeily Nia, M. Arjmand, K. Parvez, M. Naebe, *FlatChem* **2019**, 18, 100132.
- [24] N. F. Attia, S. E. A. Elashery, A. M. Zakria, A. S. Eltaweil, H. Oh, *Mater. Sci. Eng. B* **2021**, 274, 115460.
- [25] G. Huang, J. Gao, X. Wang, H. Liang, C. Ge, *Mater. Lett.* **2012**, 66, 187.
- [26] H. Nabipour, X. Wang, L. Song, Y. Hu, *Compos. A: Appl. Sci. Manuf.* **2020**, 139, 106113.
- [27] V. Unnikrishnan, O. Zabihi, M. Ahmadi, Q. Li, P. Blanchard, A. Kiziltas, M. Naebe, *J. Mater. Chem. A* **2021**, 9, 4348.
- [28] V. Unnikrishnan, O. Zabihi, Q. Li, M. Ahmadi, R. Yadav, E. N. Kalali, K. Tanwar, A. Kiziltas, P. Blanchard, D.-Y. Wang, M. Naebe, *ACS Appl. Nano Mater.* **2021**, 4(12), 13027.
- [29] M. Rubio-Martinez, C. Avci-Camur, A. W. Thornton, I. Imaz, D. MasPOCH, M. R. Hill, *Chem. Soc. Rev.* **2017**, 46(11), 3453.
- [30] H. Reinsch, S. Waitschat, S. M. Chavan, K. P. Lillerud, N. Stock, *Eur. J. Inorg. Chem.* **2016**, 2016(27), 4490.
- [31] J. Ren, X. Dyosiba, N. M. Musyoka, H. W. Langmi, M. Mathe, S. Liao, *Coord. Chem. Rev.* **2017**, 352, 187.
- [32] E.-S. M. El-Sayed, D. J. G. C. Yuan, *Green Chem.* **2020**, 22(13), 4082.
- [33] S. Kumar, S. Jain, M. Nehra, N. Dilbaghi, G. Marrazza, K.-H. Kim, *Coord. Chem. Rev.* **2020**, 420, 213407.
- [34] B. Lingesh, B. Ravikumar, B. Rudresh, D. Madhu, *Trans. Ind. Inst. Met.* **2018**, 71(3), 763.
- [35] T. Liu, X. Tian, M. Zhang, D. Abliz, D. Li, G. Ziegmann, *Compos. A Appl. Sci. Manuf.* **2018**, 114, 368.
- [36] M. Hasan, A. Abdkader, C. Cherif, F. Spennato, *Compos. A Appl. Sci. Manuf.* **2019**, 126, 105610.
- [37] O. Zabihi, M. Ahmadi, M. Naebe, *Mater. Des.* **2017**, 119, 277.
- [38] H. Unal, A. Mimaroglu, *Int. J. Polym. Mater. Polym. Biomater.* **2012**, 61(11), 834.
- [39] H. Huang, L. Yan, Y. Guo, H. L. Lin, L. Chen, L. F. Yang, Y. J. Xie, J. Bian, *Polymer* **2020**, 188, 122119.
- [40] M. Sabet, H. Soleimani, *Mater. Technol.* **2021**, 37, 1.
- [41] X. Wang, W. Cai, D. Ye, Y. Zhu, M. Cui, J. Xi, J. Liu, W. Xing, *Composites, Part B* **2021**, 224, 109206.
- [42] S. A. Seyed Esfahani, N. Ghahramani, M. Mehranpour, H. Nazockdast, *SPE Polym.* **2021**, 2(2), 134.
- [43] X. Fu, C. Yao, G. Yang, *RSC Adv.* **2015**, 5(76), 61688.
- [44] S. Satheeskumar, G. Kanagaraj, *Bull. Mater. Sci.* **2016**, 39(6), 1467.
- [45] R. Wang, Y. Zhang, X. Xie, Q. Song, P. Liu, Y. Liu, X. Zhang, *Fuel* **2021**, 285, 119161.
- [46] Y. Hou, W. Hu, Z. Gui, Y. Hu, *Indus. Eng. Chem. Res.* **2017**, 56(8), 2036.
- [47] K. A. Evans, Z. C. Kennedy, B. W. Arey, J. F. Christ, H. T. Schaefer, S. K. Nune, R. L. Erikson, *ACS Appl. Mater. Interfaces* **2018**, 10, 15112.
- [48] R. E. Lyon, R. N. Walters, *J. Anal. Appl. Pyrolysis* **2004**, 71(1), 27.
- [49] F. R. Jones, N. T. Huff, The structure and properties of glass fibers. in *Handbook of Properties of Textile and Technical Fibres*, Elsevier, Amsterdam **2018**, p. 757.

- [50] M. D. Lund, Y. Yue, *J. Am. Ceram. Soc.* **2010**, 93(10), 3236.
- [51] J. L. Thomason, C. C. Kao, J. Ure, L. Yang, *J. Mater. Sci.* **2014**, 49(1), 153.
- [52] Greenlight Surf Supply, <https://greenlightsurfsupply.com/>.
- [53] S. Kayal, A. Chakraborty, H. W. B. Teo, *Mater. Lett.* **2018**, 221, 165.
- [54] F. Jeremias, D. Fröhlich, C. Janiak, S. K. Henninger, *RSC Adv.* **2014**, 4(46), 24073.
- [55] S. Karmakar, J. Dechnik, C. Janiak, S. De, *J. Hazard. Mater.* **2016**, 303, 10.
- [56] E. Alvarez, N. Guillou, C. Martineau, B. Bueken, B. van de Voorde, C. le Guillouzer, P. Fabry, F. Nouar, F. Taulelle, D. de Vos, J.-S. Chang, K. H. Cho, N. Ramsahye, T. Devic, M. Daturi, G. Maurin, C. Serre, *Angew. Chem.* **2015**, 54(12), 3664.
- [57] N. Tannert, C. Jansen, S. Niefßing, C. Janiak, *Dalton Trans.* **2019**, 48(9), 2967.
- [58] Y. Zheng, Y. Lu, K. Zhou, *J. Therm. Anal. Calorim.* **2019**, 138(2), 905.
- [59] R. Singh, R. Kumar, I. Mascolo, M. Modano, *Composites, Part B* **2018**, 143, 132.
- [60] E. Parodi, L. Govaert, G. Peters, *Thermochim. Acta* **2017**, 657, 110.
- [61] N. Zaldua, J. Maiz, A. de la Calle, S. García-Arrieta, C. Elizetxea, I. Harismendy, A. Tercjak, A. J. Müller, *Polymer* **2019**, 11(10), 1680.
- [62] E. E. Kiziltas, H.-S. Yang, A. Kiziltas, S. Boran, E. Ozen, D. J. J. B. Gardner, *BioResources* **2016**, 11(2), 4758.
- [63] J. S. Lim, K.-i. Park, G. S. Chung, J. H. Kim, *Mater. Sci. Eng. C* **2013**, 33(4), 2131.
- [64] T. Liu, I. Y. Phang, L. Shen, S. Y. Chow, W.-D. J. M. Zhang, *ACS Publ.* **2004**, 37(19), 7214.
- [65] T. Fornes, D. R. J. P. Paul, *Polymer* **2003**, 44(14), 3945.
- [66] K. Varlot, E. Reynaud, M. Kloppfer, G. Vigier, J. J. J. O. P. S. P. B. P. P. Varlet, *Polym. Phys.* **2001**, 39(12), 1360.
- [67] H.-X. Huang, B. Wang, W.-W. Zhou, *Composites, Part B* **2012**, 43(3), 972.
- [68] S. He, J. Zhang, X. Xiao, X. Hong, Y. Lai, *J. Mater. Sci.* **2017**, 52(22), 13103.
- [69] L. Gong, B. Yin, L.-p. Li, M.-b. Yang, *Composites, Part B* **2015**, 73, 49.
- [70] A. R. Bhattacharyya, P. Pötschke, L. Häußler, D. Fischer, *Macromol. Chem. Phys. Chem. Miner.* **2005**, 206(20), 2084.
- [71] J. Liang, *J. Thermoplast. Compos. Mater.* **2011**, 24(2), 207.
- [72] G. T. Dee, B. B. Sauer, *J. Appl. Polym. Sci.* **2017**, 134(5), 44431.
- [73] G. Tsagaropoulos, A. Eisenberg, *Macromolecules* **1995**, 28(18), 6067.
- [74] C. Zhang, W. W. Tjiu, T. Liu, W. Y. Lui, I. Y. Phang, W.-D. Zhang, *J. Phys. Chem. B* **2011**, 115(13), 3392.
- [75] Q. F. Shi, H. Y. Mou, Q. Y. Li, J. K. Wang, W. H. Guo, *J. Appl. Polym. Sci.* **2012**, 123(5), 2828.
- [76] N. A. Khan, M. B. K. Niazi, F. Sher, Z. Jahan, T. Noor, O. Azhar, T. Rashid, N. Iqbal, *Polymer* **2021**, 13(14), 2307.
- [77] S. Fu, Z. Sun, P. Huang, Y. Li, N. Hu, *Nano Mater. Sci.* **2019**, 1(1), 2.
- [78] D. Elangovan, I. E. Yuzay, S. E. M. Selke, R. Auras, *Polym. Int.* **2012**, 61(1), 30.
- [79] X. Li, L. Shao, N. Song, L. Shi, P. Ding, *Compos. A: Appl. Sci. Manuf.* **2016**, 88, 305.
- [80] F. Zhao, R. Liu, X. Yu, K. Naito, X. Qu, Q. Zhang, *J. Appl. Polym. Sci.* **2015**, 132(39), 42606.
- [81] I. Inuwa, A. Hassan, D.-Y. Wang, S. Samsudin, M. M. Haafiz, S. Wong, M. Jawaid, *Polym. Degrad. Stab.* **2014**, 110, 137.
- [82] Lyon, R.; Walters, R.; Stoliarov, S., A thermal analysis method for measuring polymer flammability. In techniques in thermal analysis: Hyphenated techniques, thermal analysis of the surface, and fast rate analysis. ASTM International **2007**.
- [83] P. Zhang, L. Song, H. Lu, J. Wang, Y. Hu, *Energ. Conver. Manage.* **2010**, 51(12), 2733.
- [84] H. Chen, J. Wang, A. Ni, A. Ding, Z. Sun, X. Han, *Compos. Struct.* **2018**, 203, 894.
- [85] J. Chen, J. Wang, A. Ding, A. Ni, H. Chen, *Composites, Part B* **2019**, 179, 107555.
- [86] W. Yang, L. Song, Y. Hu, H. Lu, R. K. K. Yuen, *Composites, Part B* **2011**, 42(5), 1057.

SUPPORTING INFORMATION

Additional supporting information can be found online in the Supporting Information section at the end of this article.

How to cite this article: V. Unnikrishnan, O. Zabihi, Q. Li, M. Ahmadi, M. R. G. Ferdowsi, T. Kannangara, P. Blanchard, A. Kiziltas, P. Joseph, M. Naebe, *Polym. Compos.* **2022**, 43(9), 5877.
<https://doi.org/10.1002/pc.27002>